Undergraduate Research
Vanderbilt University, Nashville TN
Spring-Summer 2013

Flexible Parallel Robots: Constant Curvature Model

Dylan Losey

I. Introduction

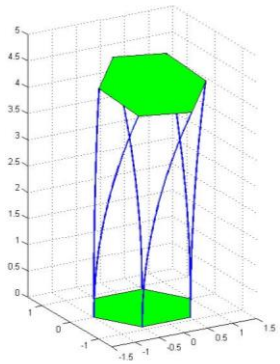

Figure 1. A sample flexible parallel robot with six legs connecting the vertices of two hexagonal platforms.

Prototypical parallel robots, such as Stewart-Gough platforms, are actuated by moving rigid legs[1]. Here we introduce, discuss, and model a parallel robot with compliant legs: a flexible parallel robot. Flexible parallel robots are defined as a set of elastic rods rigidly connected at their base ($s = 0$) and tip ($s = L$), where s is the scalar arc length parameter $s \in [0, L]$. Flexible parallel robots can thus be imagined as modified tendon robots, featuring elastic rods instead of extensible strings and a central backbone. The robots here proposed are fundamentally different from tendon-actuated robots, however, as their Grübler mobility is infinite. Given a finite number of constraints (typically determining string length), the end effector pose of a tendon-actuated robot subject to external force is fixed. Regardless of the number of constraints imposed, a flexible parallel mechanism can always translate and rotate under force without necessitating damage to the robot.

Flexible parallel robots combine many of the benefits of both parallel robots and concentric tube robots. As a result of their parallel structure these robots offer improved accuracy, rigidity, dynamic agility, and load capacity per unit mass[1,2]. Flexible parallel robots also lend themselves to miniaturization since they remove the need for external mechanisms—indeed, dexterity improves as rod radius decreases[3,4]. Device legs can be pre-curved so as to bias or increase the workspace and meet application specific requirements. We thus suggest that this design could be used to make adaptable and diminutive parallel robots modeled after traditional systems. Miniature flexible parallel robots could additionally be utilized within the field of medical robotics to make small-scale, compliant end effectors for use as wrists, camera mounts, or electro-cautery devices[5]. By stacking multiple flexible parallel robots a hybrid parallel robot can be created, offering greater workspace[6]. Finally, we contend that our design and modeling could eventually be extended to describe multiple active cannula robots acting in parallel.

In this paper we provide a constant curvature kinematic model for flexible parallel robots, find the device manipulability and compliance matrices as functions of end effector pose, and experimentally validate our model using a two-leg prototype.

II. Constant Curvature Assumption

We assume that the internal moment of each leg is instantaneously constant everywhere along the arc length of that leg. Euler-Bernoulli beam mechanics linearly relate applied moment to curvature as shown:

$\kappa = \frac{M}{EI}$; where κ is rod curvature, M is the applied moment, E is the Modulus of Elasticity and I is the cross-sectional moment of inertia

By assuming unvarying applied moment and stipulating that the rods have initially circular curvature, we can extrapolate that the legs have constant internal moment (constant preset internal moment plus constant applied moment) and accordingly bend with constant curvature. In the case of extensible string tendon-actuated robots it has been shown that the constant moment assumption described above is valid so long as the tendons are sufficiently guided[7]. The same principles apply to flexible parallel robots; if the legs are roughly parallel (i.e., at curvatures close to zero) the point force applied by each leg to the robot platform induces approximately constant moments in the other legs. Our constant curvature assumption is therefore only valid under certain design constraints. Were the legs attached to the platform using either rigid or revolute connections, the system would be over-constrained; the legs can only be orthogonal to both the robot base and platform as well as have constant curvature in certain poses. We propose using spherical joints to attach the legs to the platform and cylindrical joints to attach the legs to the base. This joint combination precludes any torsional accumulation in the rods (ignoring friction), preventing out of plant curvatures from being generated. The resultant boundary conditions of our system are listed below:

1. At its base leg i is orthogonal to the base of the robot; $Z_i(0) = Z_{i0}$, where Z_i is the 3rd column of the rotation matrix R_i
2. The position of leg i's base in the robot base frame is constant; $p_i(0)^b = p_{i0}$, where ^{b} indicates base frame
3. The position of leg i's tip in the robot platform frame is constant; $p_i(L)^p = p_{iL}$, where ^{p} indicates platform frame

III. KINEMATICS

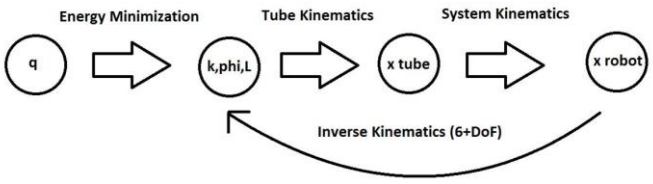

Figure 2. A diagram of the four different mechanism spaces and processes used to transform between them. Each of these processes is explained in the following sections.

Constant curvature enables a configuration space (arc parameters) which connects actuator space (leg lengths) to rod task space (rod pose). Since multiple rods are incorporated in this mechanism, we must also consider the robot task space (end effector pose). There are thus four different sets of parameters used to fully describe flexible parallel robots; the forward kinematic model designates the end effector pose as a function of leg lengths while the inverse kinematic model determines the leg lengths as a function of the end effector pose. The forward kinematic model can be further broken into three steps: leg lengths to arc parameters (joint space to rod configuration space), arc parameters to rod pose (rod configuration space to rod task space) and rod pose to end effector pose (rod task space to robot task space).

In the following section we describe each step of the forward kinematics, starting with the previously researched transformation from arc parameters to rod pose[8], next outlining the robot specific transformation from rod pose to robot pose, and then presenting the energy minimization method solution to transform joint values to arc parameters. We conclude our kinematic models by describing the simpler, but not always applicable, inverse kinematics. Though the direct kinematics are here more complicated than the inverse kinematics, as is typically the case for parallel robots, they allow for designs which aren't fully parallel and thus are essential for a general model.

A. Rod Kinematics

The rod kinematics formularize the homogeneous transformation from the rod's arc parameters to the rod's pose: $(\kappa, \phi, L)_i \rightarrow x_i$ where ϕ is the bending plane and L is the rod length. Constant curvature kinematics have previously been researched[8] and can be expressed as follows. In our notation the rod lies in the YZ plane and positive curvature corresponds to positive rotation about the X axis.

Position of a point on rod i in the base frame of that rod ^{bi}:

$$p_i(s)^{bi} = \left[0, -\frac{1}{\kappa} + \frac{1}{\kappa} * \cos(\kappa s), \frac{1}{\kappa} * \sin(\kappa s)\right]_i^T$$

Homogeneous transformation from the robot base frame to a point on rod i:

$$T(\kappa_i, \phi_i, s_i) = \begin{bmatrix} rotZ(\phi_i) & p_i(0)^b \\ 0 & 1 \end{bmatrix} * \begin{bmatrix} rotX(\kappa_i s_i) & p_i(s)^{bi} \\ 0 & 1 \end{bmatrix}$$

These formulas are ill conditioned as the rod curvature approaches zero and undefined when the rod curvature equals zero. We therefore applied L'Hopital's rule, taking partial derivatives with respect to curvature to create a piecewise definition of the rod shape:

$$p_i(s)^{bi} = \left\{ \begin{array}{l} \left[0, -\frac{1}{\kappa} + \frac{1}{\kappa} * \cos(\kappa s), \frac{1}{\kappa} * \sin(\kappa s)\right]^T \\ [0, -s * \sin(\kappa s), s * \cos(\kappa s)]^T, \ \kappa \rightarrow 0 \end{array} \right\}_i$$

This continuous piecewise definition generalizes constant curvature kinematics to account for straight rods.

B. Robot Kinematics

The robot kinematics relate the end effector pose to the pose of each rod; $(x_{i\ldots n}) \rightarrow x$ where n is the total number of legs. Robot kinematics vary from design to design. By noting that the tips of each rod lie in a plane, however, we provide an overarching method to determine specific robot kinematics. The position of an arbitrary point on the end effector in the robot base frame can be found using this equation:

$$p_{des}^b = \frac{1}{n} * \sum_{i=1}^{n} p_i(L)^b + R_p^b * \vec{a}^p$$

Where $\vec{a}^p$ is a known vector from the platform geometric center to the desired point in the platform frame and R_p^b is an SO(3) rotation matrix from the base frame to the end effector frame. This rotation matrix can be found by fitting a plane to the rod tips; first subtract the mean rod tip position (in the base frame) from each individual rod tip position (also in the base frame), then construct a 3 x n matrix composed of the resultant vectors, and finally taking the singular value decomposition of that fat matrix. The U matrix of the singular value decomposition is equivalent to the rotation matrix from robot base to the plane in which the end effector lies (R_p^b).

C. Energy Minimization

We utilized an energy minimization argument to determine each rod's complete arc parameters given all rod lengths: $L_{i\ldots n} \rightarrow (\kappa, \phi, L)_{i\ldots n}$. We here assume that the system is adiabatic[3] and as such the rods will bend and rotate so as to maintain the lowest energy state possible. Noting that these kinematics describe only static systems, the total energy of a rod is equal to the sum of the rod's torsional energy and bending energy. The torsional energy of each rod is zero since the rod is free to rotate at the base (cylindrical joint) and rotationally unconstrained at the tip (spherical joint). We thus write the energy of rod i as follows:

$$U_{i,bend} = \frac{(EI * L)_i}{2} * (\kappa_i - \kappa_{i,home})^2$$

The total energy of the robot is simply the sum of the bending energy of each component rod. If the system were unconstrained the total energy of the robot is at a minimum when $\kappa_{1\ldots n} = \kappa_{1,home\ldots n,home}$. Because the rod tips are rigidly connected, however, the system is frequently prevented from attaining this configuration. The rods therefore bend and rotate subject to a set of positional constraints imposed by the platform boundary condition.

Given that the length of each rod can be found from actuator values using a robot specific conversion, there exist $2n$ unknown arc parameters $(\kappa_{1\ldots n}, \phi_{1\ldots n})$. The number of constraints depends on the number of legs. If the robot is under-actuated (2-5 legs), there must be more unknowns than constraints; if the robot is fully parallel (6 legs), there exist an equal number of unknowns and constraints; if the robot is redundant (7+ legs), then the number of positional constraints

exceeds the number of unknowns. We use two different methods to determine the number and nature of these constraints. For mechanisms with two to four DoF we use the combination formula (n choose 2) to determine the number of scalar distances needed to connect every rod tip. For mechanisms with five or more legs we determine the 2 x 1 vectors from an arbitrarily selected rod tip to every other rod tip and then impose a planar constraint. Changing methodologies as described allows us to reduce the constraints.

Number of Legs	Number of Unknown Arc Parameters	Minimum Number of Constraints
2	4	1
3	6	3
4	8	6
5	10	9
6	12	12

Table 1. The number of constraints necessary to define the system and satisfy the requirements of the Lagrange multipliers method. When the robot is fully parallel, the Lagrange multipliers method can no longer be applied but inverse kinematics become possible.

Our goal is to find the unknown arc parameters $(\kappa_{1..n}, \phi_{1...n})$ that minimize the total energy function $U(\kappa_{1...n})$ subject to these positional constraints $f(\kappa_{1...n}, \phi_{1...n}) = 0$. For example, the total energy of a two-leg mechanism can be expressed as follows:

$$U_{1,bend} = \frac{(EI * L)_1}{2} * (\kappa_1 - \kappa_{1,home})^2$$

$$U_{2,bend} = \frac{(EI * L)_2}{2} * (\kappa_2 - \kappa_{2,home})^2$$

$$U(\kappa_1, \kappa_2) = U_{1,bend} + U_{2,bend}$$

and the distance positional constraint is as follows:

$ceq = \|p_1(L)^b - p_2(L)^b\|$, where ceq denotes equality constraint

$$f(\kappa_1, \kappa_2, \phi_1, \phi_2) = \|p_1(L)^b - p_2(L)^b\| - ceq = 0$$

To find the unknown arc parameters $(\kappa_1, \kappa_2, \phi_1, \phi_2)$ we use Lagrange multipliers for constrained optimization. We have $2n = 4$ unknowns and $r = 1$ constraint, and since $2n > r$ multiple solutions exist. Based on the two-leg example, the system of equations resulting from the Lagrange multipliers method is shown below:

$$L(\kappa_1, \kappa_2, \phi_1, \phi_2, \lambda) = U(\kappa_1, \kappa_2) + \lambda * f(\kappa_1, \kappa_2, \phi_1, \phi_2)$$

$$\frac{\partial L}{\partial \kappa_1} = \frac{\partial U(\kappa_1, \kappa_2)}{\partial \kappa_1} + \lambda * \frac{\partial f(\kappa_1, \kappa_2, \phi_1, \phi_2)}{\partial \kappa_1} = 0$$

$$\frac{\partial L}{\partial \kappa_2} = \frac{\partial U(\kappa_1, \kappa_2)}{\partial \kappa_2} + \lambda * \frac{\partial f(\kappa_1, \kappa_2, \phi_1, \phi_2)}{\partial \kappa_2} = 0$$

$$\frac{\partial L}{\partial \phi_1} = \lambda * \frac{\partial f(\kappa_1, \kappa_2, \phi_1, \phi_2)}{\partial \phi_1} = 0$$

$$\frac{\partial L}{\partial \phi_2} = \lambda * \frac{\partial f(\kappa_1, \kappa_2, \phi_1, \phi_2)}{\partial \phi_2} = 0$$

$$\frac{\partial L}{\partial \lambda} = U(\kappa_1, \kappa_2) + f(\kappa_1, \kappa_2, \phi_1, \phi_2) = 0$$

There are now $2n + r$ equations and $2n + r$ unknowns; the solution to this system of equations includes the desired arc parameters. The energy minimization method thus allows us to determine the complete arc parameters of every rod given the initial lengths of those rods and the geometry of the mechanism. It should be noted, however, that while this method can be used to mathematically calculate multiple equivalent minima, it does not provide any intuition as to which of these equally likely arc parameters the mechanism will actually attain. In situations where several minimum energy solutions exist we favor the projection with the least total change in rod bending plane and assume hysteresis and bifurcation do not affect the legs.

D. Inverse Kinematics

Inverse kinematics can be used to find every rod's arc parameters and—using a robot specific relationship—the actuator values necessary to attain a desired pose: $x \rightarrow (\kappa, \phi, L, q)_i$. A mechanism must have six DoF to guarantee a unique inverse kinematics solution as a desired pose may or may not exist in an under-actuated robot's workspace. By means of the loop closure method we can find the vector from the base to tip of rod i:

$$p_{plat}^b + R_p^b * p_i(L)^p - p_i(0)^b = [\Delta x \quad \Delta y \quad \Delta z]_i^T$$

where p_{plat}^b and R_p^b are given (end effector pose in the base frame). Here we note that the vector connecting the base and tip of rod i lies in the bending plane of rod i:

$$\phi_i = atan2(\Delta x_i, -\Delta y_i)$$

We subsequently redefine the vector components such that they are consistent with our rod frame:

$\Delta h_i = -\|\langle \Delta x \quad \Delta y \rangle_i^T\|$; where Δh describes the horizontal displacement of the rod

$\Delta v_i = \Delta z_i$; where Δv describes the vertical displacement of the rod

Recalling the constant curvature assumption and recognizing that these displacements describe the position of a point on the rod where $s = L$, we can write a system of equations to determine the rod arc parameters:

1. $\Delta h_i = \left(-\frac{1}{\kappa} + \frac{1}{\kappa} * \cos(\kappa L)\right)_i \; or \; \Delta h_{i,\kappa \rightarrow 0} = (-L * \sin(\kappa L))_i$

2. $\Delta v_i = \left(\frac{1}{\kappa} * \sin(\kappa L)\right)_i \; or \; \Delta v_{i,\kappa \rightarrow 0} = (L * \cos(\kappa L))_i$

When solved simultaneously, the above equations provide the curvature and length of rod i. The inverse kinematics are thus obtained from purely geometric arguments relying on both our constant curvature assumption and rod kinematics.

E. Model Comparison

Instead of using Euler-Bernoulli beam mechanics, the kinematics of a flexible parallel robot could be derived using Cosserat rod mechanics. This Cosserat rod model would remove the need for any constant curvature assumption and as such allow for more diverse and accurate modeling[9,10,11]. If the conditions for our constant curvature assumption are met, however, the model predictions for both Euler-Bernoulli and Cosserat rod mechanics are very similar. For instance, in the case of a two-leg mechanism with zero pre-curvature in each leg and a constraint distance α between the rod ends, the norm of the predicted positional difference between both models is less than $(1e-2)/\alpha$ so long as the difference in rod lengths is equal to or less than α. The models increasingly diverge as the constant curvature assumptions become inapplicable, i.e., when the legs reach higher curvatures or have a greater disparity in curvatures. Implementation of the Cosserat rod

model is more computationally expensive than the kinematic model presented here—we estimate that the constant curvature kinematics take less than 0.05 sec to run in MATLAB, while the Cosserat rod code developed by Rucker takes more than 1.75 sec to run on the same machine.

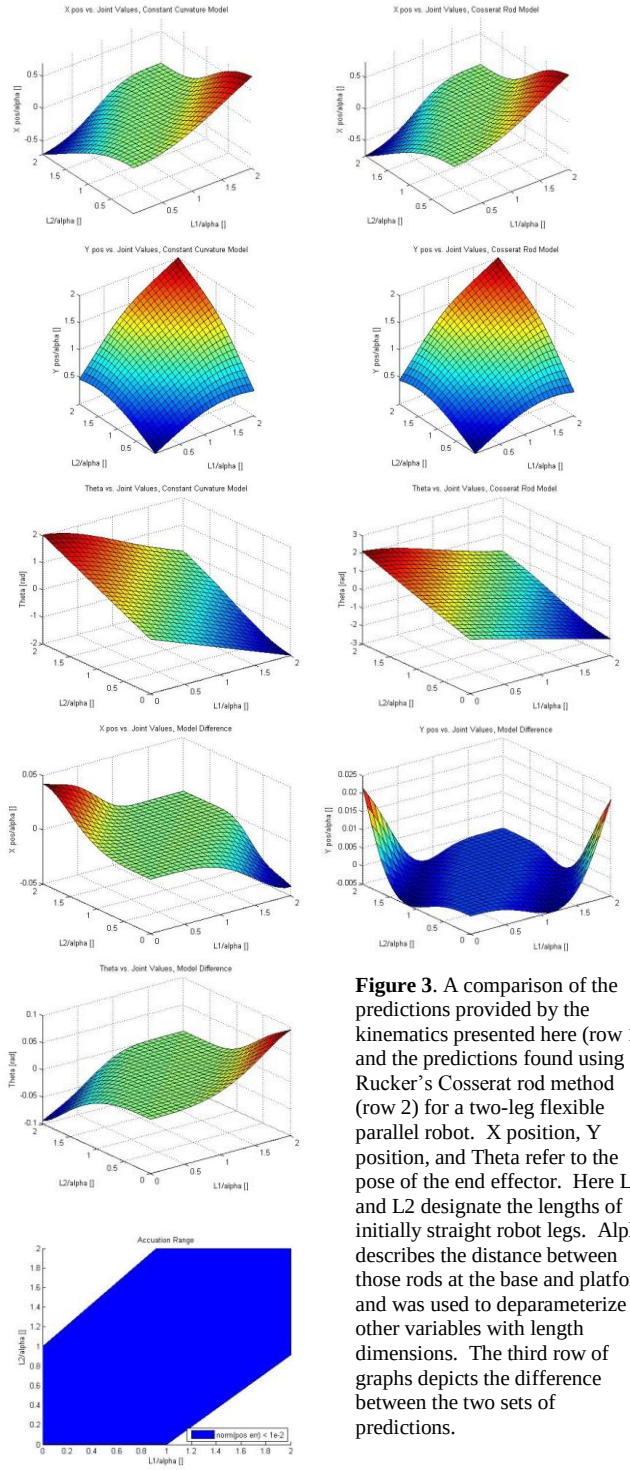

Figure 3. A comparison of the predictions provided by the kinematics presented here (row 1) and the predictions found using Rucker's Cosserat rod method (row 2) for a two-leg flexible parallel robot. X position, Y position, and Theta refer to the pose of the end effector. Here L1 and L2 designate the lengths of initially straight robot legs. Alpha describes the distance between those rods at the base and platform and was used to deparameterize other variables with length dimensions. The third row of graphs depicts the difference between the two sets of predictions.

Figure 4. The set of leg lengths at which the distance between our constant curvature kinematic model of end effector position and Rucker's Cosserat rod model of end effector position is less than $(1e-2)/\alpha$. This actuation range encourages greater tube offsets.

IV. Jacobian and Compliance Matrices

A. Jacobian

The spatial manipulator Jacobian for a mechanism is defined as follows:

$$J^s = \left[\left(\frac{\partial gst}{\partial L_1} gst^{-1}\right)^\vee \quad \cdots \quad \left(\frac{\partial gst}{\partial L_n} gst^{-1}\right)^\vee\right]$$

where gst is the homogeneous transformation from base frame to end effector frame and $\frac{\partial gst}{\partial L_i}$ is the change in gst as rod i is actuated. Given a complete set of leg lengths gst can be computed solely using the direct kinematics derived in the previous section. This homogeneous transformation is necessarily numeric, however, since implementation requires functions such as `fmincon`; we consequently estimate the partial derivative terms $\left(\frac{\partial gst}{\partial L_i}\right)$ by means of the finite difference approximation. Applying finite differences the spatial manipulator Jacobian is rewritten as[10,12]:

$$J^s \approx \left(\frac{gst(L_1+\Delta L) - gst(L_1-\Delta L)}{2\Delta L} gst^{-1}\right)^\vee \ldots \left(\frac{gst(L_n+\Delta L) - gst(L_n-\Delta L)}{2\Delta L} gst^{-1}\right)^\vee$$

and may later be transformed so as to obtain either the hybrid or body Jacobian. The exactness of the resultant Jacobian depends on both the size of ΔL and the accuracy of the constant curvature assumption. The Jacobian can be used to direct resolved rates control of the mechanism.

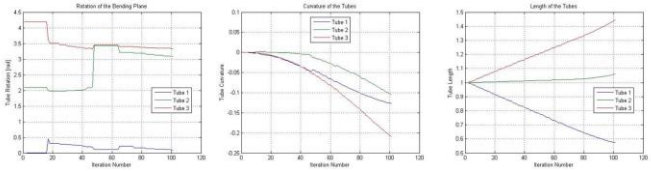

Figure 5. Sample plots resulting from a resolved rates algorithm based on the Jacobian derived in this section. Though the leg lengths and curvatures changed fairly consistently the rod bending plane of this three-leg robot rapidly shifted to attain lower energy configurations.

B. Compliance Matrix

Much like the spatial Jacobian, the spatial manipulator compliance matrix with respect to a tip wrench (Wr) is defined as:

$$C^s = \left[\left(\frac{\partial gst}{\partial Wr_1} gst^{-1}\right)^\vee \quad \cdots \quad \left(\frac{\partial gst}{\partial Wr_6} gst^{-1}\right)^\vee\right]$$

where $\frac{\partial gst}{\partial Wr_i}$ is the change in gst as wrench component i is altered. In order to calculate the partial derivative terms $\left(\frac{\partial gst}{\partial Wr_i}\right)$, we here formularize $gst(L, Wr)$ utilizing Castigliano's Theorem. Castigliano's Theorem defines the deformed position of a rod subject to an external wrench by relating strain energy and generalized force; these equations do not assume that the deformed rod maintains constant curvature and as such offer superior prediction accuracy. In realistic cases the rod radius ($R = 1/\kappa$) of our mechanism will be significantly greater than the rod thickness. Thus, the rod's eccentricity is negligible and its strain energy can be written:

$$U_i = \left(\frac{R}{2EI}\int_0^{kL} m(\theta)^2\, d\theta\right)_i$$

where $m(\theta)$ is the internal moment of the rod as a function of θ, the in-plane angle ($\theta = \kappa s$).

According to Castigliano's Second Theorem, the deflected position of rod i is equivalent to the partial derivative of rod i's strain energy with respect to the forces applied on that rod (F_i):

$\vec{\delta}_i(F_i)^{lcf} = \frac{\partial U_i}{\partial F_i} = \begin{bmatrix}\frac{\partial U_i}{\partial F_{ix}} & \frac{\partial U_i}{\partial F_{iy}} & \frac{\partial U_i}{\partial F_{iZ}}\end{bmatrix}^T$, where lcf denotes local frame

We note that as rod curvature approaches zero this simplifies to the Euler-Bernoulli formula for cantilever beams under end loading as follows:

$$\vec{\delta}_i(F_i)^{lcf}{}_{\kappa\to 0} = \begin{bmatrix}\frac{F_x L^3}{3EI} & \frac{F_y L^3}{3EI} & \frac{F_z L^3}{3EI}\end{bmatrix}_i^T$$

The internal moment of the rod (m) is found through manipulating constant curvature geometry and arc parameter relations[13]. Let's take the two-leg mechanism we discussed in the energy minimization section as an example; the internal moment at a point along the rod i is equal to the sum of the rod's initial internal moment (m_x)—which is here constant throughout the circular rod—plus any internal moments caused by the applied tip force $\left(m_{F_y}(\theta),\ m_{F_z}(\theta)\right)$ evaluated at the selected angle:

$$m_i(\theta) = \left(m_x + m_{F_y}(\theta) + m_{F_z}(\theta)\right)_i$$

The initial bending energy of the constant curvature rod is simply expressed using Euler-Bernoulli mechanics:

$$m_x = M_{x,rod} = EI\Delta\kappa,\ \Delta\kappa = \kappa - \kappa_{home}$$

while the moments due to tip forces are assessed by constructing a right triangle connecting the rod base, rod tip, and projection of the rod tip onto the Y axis. The moment arms can then be calculated using trigonometry and the in-plane bending angle:

$$m_{F_y}(\theta) = F_y * R * \sin(\theta)$$
$$m_{F_z}(\theta) = F_z * R * (1 - \cos(\theta))$$

Though we have now completely defined Castigliano's method as pertains to our mechanism, we cannot implement these formulas without knowing the forces applied to each rod $\left(F_x, F_y, F_z\right)_i$. We solve a system of equations to determine these forces applied to each rod tip—or negative reaction forces of each rod tip—for a given wrench.

A mechanism with two legs (planar) has four unknown reaction forces (two for each leg), while a mechanism with three or more legs (3D) has $3i$ unknown reaction forces. Provided a known external wrench, the forces acting on each rod tip must satisfy three general sets of constraints: force, moment, and position. The sum of the force components acting on each rod tip in the tool frame must equal the applied wrench force components; this provides two constraints in the planar case or three constraints in the 3D case. The sum of the moment components acting on each rod tip in the tool frame must likewise equal the applied wrench moment components; this provides one constraint in the planar case or three constraints in the 3D case. Finally, the deformed position of each rod tip must satisfy the positional constraints imposed by the platform—the number, nature and value of these constraints are identical to those found while determining the direct kinematics. It should be noted that the sum of the force, moment, and position constraints for a two- to six-leg robot equals the number of unknowns.

The deformed position of a rod tip is equal to the deformed rod tip vector, found by applying Castigliano's method as previously described, plus the initial rod tip position vector. When solving for the forces applied to each rod tip, we must iteratively calculate the deformed position of the rod; as such, in the process of finding the applied forces we also find the desired homogeneous transformation from base frame to tip frame of a mechanism with given leg lengths and a specified applied wrench. To better illustrate this process we return to our two-leg example. For a given wrench in 2D space $Wr = [F_y \quad F_z \quad M_{x,plat}]^T$ there exist four unknowns $F_1 = \begin{bmatrix}F_{1y}\\F_{1z}\end{bmatrix}$, $F_2 = \begin{bmatrix}F_{2y}\\F_{2z}\end{bmatrix}$; the constraint equations (position, force, and moment) are thus:

1. $ceq = \|p_1'(L)^b - p_2'(L)^b\|,\ p_1'(L)^b = p_1(L)^b + \vec{\delta}_1(F_1)^b$ and $p_2'(L)^b = p_2(L)^b + \vec{\delta}_2(F_2)^b$
2. $F_{1y} + F_{2y} = F_y$
3. $F_{1z} + F_{2z} = F_z$
4. $M_{x,plat} = -\Delta z * F_{2y} + \Delta y * F_{2z}$, $[\Delta x \quad \Delta y \quad \Delta z]^T = p_2'(L)^b - p_1'(L)^b$

We guess the reaction forces of each rod and then check that the forces and moments balance. We then use Castigliano's method to find the deformed position of each rod given our reaction force guesses; we finally check to see if the new position of each rod tip satisfies the mechanism geometry. Since the number of constraints here equals the number of unknowns we can simultaneously solve for both the force acting on each rod tip and $gst(L, Wr)$. When executing this series of steps—we used `fsolve` or `fmincon` with an interior point algorithm—the solution is again necessarily numeric, and as such we approximated the compliance matrix using the method of finite differences[10,12]:

$$C_i^s \approx \left(\frac{gst(Wr_i + \Delta Wr) - gst(Wr_i - \Delta Wr)}{2\Delta Wr} gst^{-1}\right)^{\vee},\ i = 1 \ldots 6$$

The resultant spatial compliance matrix with respect to a tip wrench can be transformed into the body compliance matrix, hybrid compliance matrix, or stiffness matrix ($K = C^{-1}$) as needed.

C. *Ellipsoid Maps*

The singular value decomposition of the first three rows of the Jacobian matrix yields both the semi-principal axes lengths and the SO(3) rotation matrix of the positional manipulability ellipsoid. This ellipsoid indicates the ability of the end effector to be driven in a direction via joint actuation at the current leg lengths. When all mechanism legs have zero curvature and are the same length, the robot is in a singularity; we mathematically avoid these singularities by using this singularity-robust pseudo-inverse formula[2]:

$\dot{L}_{des} = J^T(JJ^T + \rho I)^{-1}\dot{x}_{des}$, where ρ is a user selected small scalar ($\approx 1e-2$)

The translational manipulability of the mechanism generally increases as the difference in rod curvatures increases. Likewise, the singular value decomposition of the relevant

portion of the compliance matrix (rows 1:3, columns 1:3) yields both the semi-principal axes lengths and the SO(3) rotation matrix of the positional compliance ellipsoid. This ellipsoid indicates the ability of the end effector to be pushed in a direction via an external wrench at the current leg lengths. The translational compliance ellipsoid and the translational stiffness ellipsoid are usually at or near singularity because the mechanism is much more compliant to applied forces normal to the legs than applied forces parallel to the legs.

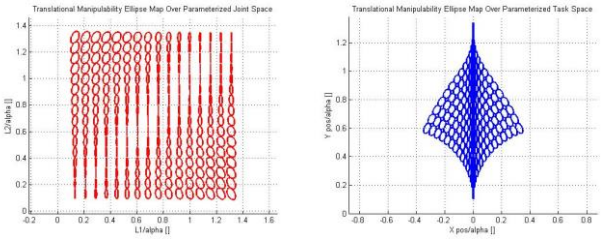

Figure 6. Sample scaled translational manipulability ellipse maps over both joint space and workspace. These plots were simulated with a two-leg, zero precurvature flexible parallel robot.

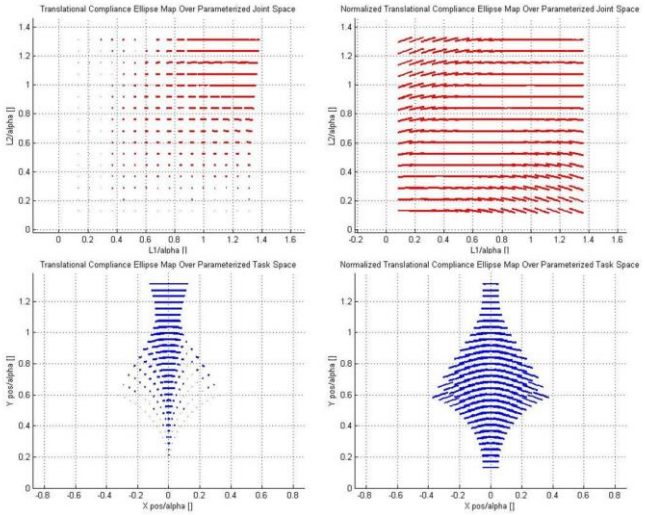

Figure 7. Sample scaled translational compliance ellipse maps over both joint space and workspace. These plots were simulated with a two-leg, zero precurvature flexible parallel robot. Both columns were created with the same mechanism, but the ellipses graphed in the second column have been normalized to better show their orientation.

V. Validation of Direct Kinematics

A. Experimental Setup

In order to test our kinematic model we constructed a prototype two-leg flexible parallel robot. The legs were composed of solid 1.8 mm diameter nitinol wire with zero precurvature and were fastened to the platform by means of plastic spherical joints (McMaster 1071K11). Both the base and platform were laser-cut from acrylic; the platform and spherical joints had been modified to provide greater than 215^0 and 107.5^0 swivel on the right and left legs respectively. The legs were rigidly attached to and actuated by a pair of linear sliders with sub-millimeter accuracy. The entire mechanism was mounted horizontally on a lubricated surface to avoid un-modeled effects of gravity on the rods and platform.

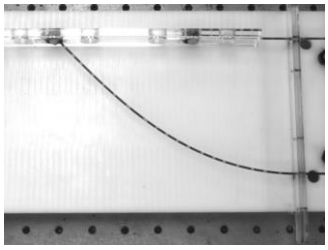

Figure 8. Image from our experimental validation of the constant curvature kinematic model. The base platform, legs, spherical joints and end effector are pictured here using one of the two stereo cameras as the robot takes a near 90^0 orientation.

During experiments we turned the sliders to set a variety of known leg lengths. We then photographed the base, rods, and platform of the robot with two calibrated cameras and used stereo vision to extract user-selected 3D points. Prior to the experiment a series of hash marks had been placed on each rod; after the experiment we selected the midpoint of each corresponding hash mark on both right and left camera photos and determined the position of the designated point. The hash marks were irregularly spaced but resulted in points measured every ten to twenty millimeters. The cumulative error of our stereo vision system was approximately less than or equal to one millimeter (the exact amount of human error in selecting points is unknown). After we had mapped the rod shape we fit a plane to our points and used the U singular value decomposition matrix to rotate those points into our YZ rod frame. To find the radii of the measured points, we fit a circle to each rod and mandated that the point corresponding to the base of that rod lies on the circle.

B. Results

The results of our experiments are shown in the figures below. Here $alpha$ refers to the distance between the rods at the base and platform, $L1$ refers to the length of the left leg and $L2$ refers to the length of the right leg. The predicted mechanism shape is shown in green while the measured points and platform line are shown in blue. It should be noted that while we here used the conventional XY frame for simplicity, we would typically mark these graphs using YZ axes.

During the ten experiments conducted with our two rod prototype the average distance between predicted end effector position and actual end effector position was $2.65\ mm$; the average difference between predicted end effector orientation and actual end effector orientation was 0.737^0; the average difference between predicted radius of the left leg (more curved) and actual radius of the left leg was $18.55\ mm$. As δL—the variation in leg lengths—increased the positional error increased, the rotational error was unchanged, and the radius error decreased. More conclusive results would have been obtained had more experiments been conducted, but we expect that the positional and rotational error will rise as δL increases and the mechanism diverges from constant curvature. The leg radius error may actually improve as curvature increases because slight discrepancies at lower curvatures are magnified.

VI. Conclusion

Here we have introduced flexible parallel robots—a novel robot design—and performed preliminary kinematic and compliance modeling. Although the constant curvature assumption necessary for these kinematic models prohibits

certain robot constructions, our experiments have shown that for simple cases this assumption accurately and efficiently predicts rod shape and end effector pose. Using only the work we have presented, others could construct miniature end effectors and cheap parallel robots.

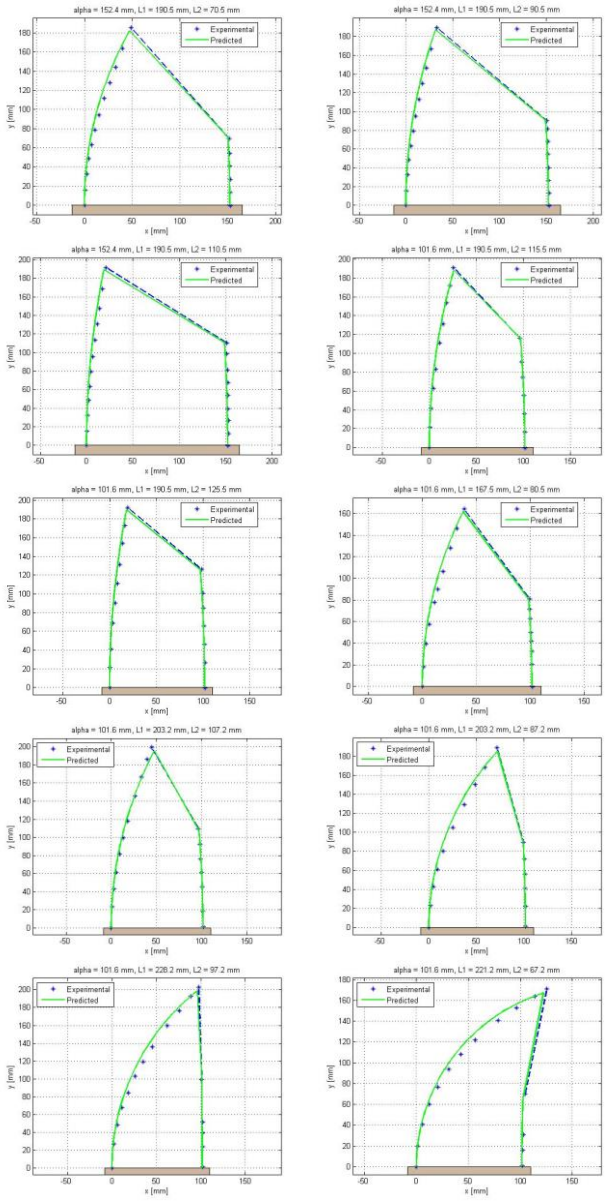

Figure 9. Results from ten sets of experiments using two different values of α and assorted sets of leg lengths. With these graphs we seek to highlight the close alignment between the predicted rod and platform pose and the measured rod and platform pose. The parallel structure aids our predictions by reducing the cumulative errors in rod pose. As δL increases the rods appear to increasingly diverge from circular arcs.

Acknowledgements

I'd like to thank Professor Webster for the opportunities and encouragement he provided during my first steps in the field of robotics. I'd also like to thank the graduate students working in the MED Lab, particularly my advisor Richard Hendrick, for their help and kindness throughout my research.

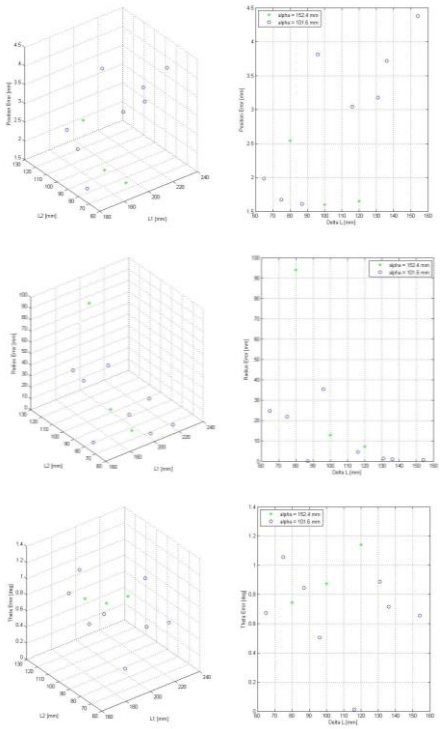

Figure 10. Plots of the end effector positional error, orientation error, and the bent rod's radius error, where error is defined as the difference between experimental and predicted. These plots summarize the results of our experiments and reveal some general patterns in model behavior, as described in the results section.

References

[1] Merlet, J.-P. "Introduction, structural synthesis and architectures." *Parallel Robots*. 2nd ed. Dordrecht: Springer, 2006.
[2] Simaan, N. Lecture notes. Robotic Manipulators ME331. Vanderbilt University, Nashville, TN. Spring 2013.
[3] Webster III, R. J. Design and mechanics of continuum robots for surgery. Diss. Johns Hopkins University, 2007.
[4] Webster III, R. J., Romano, J. M., and Cowan, N. J. Mechanics of precurved-tube continuum robots. *IEEE Transactions on Robotics* **25**(1), 67-78 (2009).
[5] Losey, D. L., York, P. A., Swaney, P.J., Burgner, J. and Webster III, R. J. A flexure-based wrist for needle-sized surgical robots. *SPIE Medical Imaging*, 2013.
[6] Charentus, S. and Renaud, M. Modeling and control of a modular, redundant robot manipulator. *Lecture notes in control and information sciences* **139**, 508-527 (1990).
[7] Li, C. and Rahn, C. Design of continuous backbone, cable-driven robots. *ASME Journal of Mechanical Design*, **124**(2), 265-271 (2002).
[8] Webster III, R. J. and Jones., B. A. Design and kinematic modeling of constant curvature continuum robots: a review. *International Journal of Robotics Research* **29**(13), 1661-1683 (2010).
[9] Antman, S. S. *Nonlinear Problems of Elasticity*. 2nd ed. New York: Springer, 2005.
[10] Rucker, D. C. The mechanics of continuum robots: model-based sensing and control. Diss. Vanderbilt University, 2011.
[11] Rucker, D. C. and Webster III, R. J. Statics and dynamics of continuum robots with general tendon routing and external loading. *IEEE Transactions on Robotics* **27**(6), 1033-1044 (2011).
[12] Rucker, D. C. and Webster III, R. J. Computing Jacobians and compliance matrices for externally loaded continuum robots. *IEEE International Conference on Robotics and Automation*, 945-950 (2011).
[13] Budynas, R. G., Nisbett, J. K. and Shigley, J. E. *Shigley's Mechanical Engineering Design*. 9th ed. New York: McGraw-Hill, 2011.